A Study on the Selectivity of Toluene/Ethanol Mixtures on the Micellar and Ordered Structures of Poly(styrene-*b*-4-vinylpyridine) Using Small-angle X-ray Scattering, Generalized Indirect Fourier Transform, and Transmission Electron Microscopy

Soo-Young Park,* Woo-Hwan Sul, and Yun-Jeong Chang

Department of Polymer Science, Kyungpook National University, #1370 Sangyuk-dong, Buk-gu, Daegu 702-701, Korea

Received January 2, 2007; Revised Manuscript Received March 16, 2007

ABSTRACT: The effects of the selectivity of toluene/ethanol mixtures on the micellar and ordered structures of PS(12K)-*b*-P4VP(11.8K) in the dilute, semidilute, and concentrate solutions, as well as in the solid state, were studied using small-angle X-ray scattering (SAXS), generalized indirect Fourier transform (GIFT), and transmission electron microscopy (TEM) methods. For the dilute solutions (1 wt %), only form factors were observed in SAXS at ϕ (weight percent of ethanol in the ethanol/toluene mixture) = 0 to 20 and 70 to 100 (selective solvents), while isotropic states were found at other solvent mixture ratios (nonselective solvents). Hard and large spherical micelles were formed in high-selective solvent mixtures while soft and small ones were formed in less-selective solvent mixtures. For the semidilute solution (8 wt %), both of structure and form factors of SAXS curves appeared in selective solvents while isotropic states were also observed in nonselective solvents. The form factors that were separated by using GIFT were similar to those from the dilute solution. For the concentrated solution (16 wt %), new soft micelles, which were in an isotropic state in the dilute and semidilute solutions, were formed in nonselective solvents by increasing the concentration of the solution to 16 wt %. The cubic packing of spherical micelles could be observed in entire solvent mixtures, except for the solution at $\phi = 40$, which had two-dimensional hexagonal packing. Hard micelles favored a fcc symmetry, although soft micelles favored a bcc symmetry. During drying from the 16 wt % solution to a solid state, hard spherical micelles remained and were randomly packed although soft micelles were transformed into thermodynamically stable lamellar structures. The hexagonally packed structures at $\phi = 40$ maintained their original hexagonal packing after drying. The various structures for PS(12K)-*b*-P4VP(11.8K), such as hard/soft spherical micelles in the dilute solution, fcc, bcc, and hexagonal packing in the concentrate solution, and randomly packed micellar, lamellar, and hexagonal structures in the solid state, could be finely tuned by using a simple toluene/ethanol mixture in this study.

Introduction

Block copolymers are one of the most valuable classes of polymeric materials due to their ability to self-assemble, either in bulk or in selective solvents, thus leading to characteristic morphologies in bulk, and to micelle formations in selective solvents.[1] The micelles in selective solvents consist of a core and their surrounding protective corona, which is formed by insoluble and soluble blocks, respectively.[2] The insoluble block minimizes contact with the solvent and favors micelle formation. The resulting micelles can access a wide range of morphologies such as spheres, rods, vesicles, lamellae, large-compound micelles, nanofibers, and nanotubes.[3−9] The morphology of micelles is dependent on several variables, such as block copolymer composition and concentration,[10] the type and concentration of added ions,[11,12] and the selectivity of the solvent.[13,14] Force balances among the stretching of core blocks, the repulsive interaction among corona chains, and surface tension of the core/corona interface at the onset of micellization, mainly control these morphologies.[13,15] The Flory interaction parameter between constituent blocks (χ), the molecular weight and composition of each block and solvent selectivity mostly determine morphology in bulk, as well as in a solution state. However, intrinsic properties such as χ, and the molecular weight and composition of each block are not readily tunable factors for a given block copolymer system, although solvent selectivity can be easily adjusted. Pioneering researches has been conducted by the Eisenberg group, who investigated poly(styrene-*b*-acrylic acid) (PS-*b*-PAA) ionic diblock copolymers in water/dioxane or water/dimethylformamide (DMF) mixtures.[16−20] They observed transitions from spheres, to cylinders and to vesicles by increasing the amount of water in the mixture, thereby increasing interfacial tension.

The poly(styrene-*b*-4-vinylpyridine) (PS-*b*-P4VP) used in this study is a class of nonionic, amphiphilic block copolymers, which has been of great interest in the study of micellar properties. This is due to its high quality and relatively easy access to commercially available block copolymers. In addition, the same refractive index of each block polymer simplifies the evaluation of light scattering data, and the sufficiently different solution properties of PS and P4VP in block copolymers allow for the formation of micelles in most solvents.[21] Furthermore, due to the presence of a strong absorbing block, PS-*b*-P4VP has been often used to study adsorption on to solid surfaces.[22] PS-*b*-P4VP is in a strongly segregated regime, its critical micelle concentration (cmc) is very low, and the size of the micelles remained unchanged in concentrations ranging from 10^{-3} to 5×10^{-3} g/mL.[23]

Recently, we reported on the structure of the micelles and their ordered structures of PS-*b*-P4VP in a toluene solution.[24] In the current study, the effects of selectivity of toluene/ethanol mixtures on the micellar and ordered structures of PS(12K)-*b*-P4VP(11.8K) in the dilute, semidilute, and concentrate solutions

* To whom correspondence should be addressed. Telephone: +82-53-950-5630. Fax: +82-53-950-6623. E-mail psy@knu.ac.kr.

10.1021/ma0700072 CCC: $37.00
Published on Web 04/18/2007

as well as in the solid state, were studied using small-angle X-ray scattering (SAXS), generalized indirect Fourier transform (GIFT), and transmission electron microscopy (TEM) methods. This was done in order to clarify the influence of the nature of block-selective solvents on the morphology of resulting micelles in a binary solvent mixture of toluene (PS selective solvent) and ethanol (P4VP selective solvent). Not only were the structures of the individual micelles studied but also their packing in mixture solvents was examined at the synchrotron radiation source.

Experimental Section

Samples. PS-*b*-P4VP was purchased from Polymer Source, Inc. (Canada) and was synthesized by an anionic polymerization method. Toluene and ethanol were used as selective solvents for the PS and P4VP blocks, respectively. Two solvents were mixed by weight percent in order to control the selectivity of the solvent. The ethanol content in the toluene/ethanol mixture was expressed as ϕ in weight %. The solution samples were prepared by the direct dissolution of polymers in the solvent. The number-average molecular weight was 12000/11800 (PS/P4VP) (PS(12K)-*b*-P4VP-(11.8K)) in g/mol and its polydispersity was 1.04. Copolymers were dissolved in mixture solvents at concentrations of 1, 8, and 16 wt %. The solid film was prepared by drying a 16 wt % solution between PET films in open air. The ultrathin film of the solid-state sample was sectioned by an ultramicrotome (Leica EM UC6). The TEM samples (Hitachi H-7600, 100 kV) were also prepared by dropping solutions on to a 200-mesh carbon-coated copper grid, the solvent was absorbed on filter paper, and the solvent was evaporated at room temperature. The grid samples were stained with I_2 vapors for 90 min.

Small-Angle X-ray Scattering (SAXS). The sample holder for SAXS has a mica window and a hole for the injection of the solution. The hole of the sample holder was sealed with epoxy after the solution was injected. This was done in order to prevent the solvent from evaporating during SAXS measurements. SAXS experiments during evaporation from the 16 wt % toluene and ethanol solutions to the solid state in the synchrotron were performed by taking out the 16 wt % solution (in the gel state) from the sealed sample vial, immediately putting it on the mica in the sample holder, and then shooting X-rays as soon as possible. The frames were recorded every 5 s until the SAXS patterns did not change. The scattering pattern of the last frame during evaporation was almost identical to the frame after 1 day, indicating that the samples were completely dried during the experiment. Experiments were performed at beamline 4C1 (the Pohang Light Source, Korea), where a W/B4C double-multilayer monochromator delivered monochromatic X-rays that had a wavelength of 0.16 nm. A flat Au mirror was used to reject higher harmonics from the beam. A MarCCD camera (Mar USA, Inc. CCD165) was used to collect the scattered X-rays. The sample-to-detector distance (sdd) was 3 m, which allowed SAXS data to be obtained in a q range between 0.06 and 1.11 nm^{-1} (sdd = 3 m). The sdd was calibrated using SEBS (polystyrene-*block*-poly(ethylene-*ran*-butylene)-*block*-polystyrene).

Data Analysis

The raw spectra were corrected for the background of the solvent and sample cell and detector efficiency by conventional procedures. Two-dimensional scattering spectra were azimuthally averaged. The measured intensity $I(q)$ can be expressed as the product of form ($F(q)$) and structure ($S(q)$) factors, although $S(q)$ is negligible for the dilute solution. SAXS data were analyzed with GIFT software, which was developed by Glatter.[25−31] Both $F(q)$ and $S(q)$ were determined simultaneously within one procedure in GIFT. While $F(q)$ is absolutely model free, $S_{avg}(q)$ is calculated within the Percus−Yevick approximation and is not model independent. Fourier transformation of the $F(q)$ yields pair distance distribution function ($p(r)$) of a particle, which is a histogram of distances inside the particle weighted with electron density differences. The shape of the $p(r)$ allowed the determination of basic geometry (spherical, cylindrical, or planar), even for inhomogeneous particles. This methodology, using indirect Fourier transformation, has been described elsewhere.[25−31] D_{max} was determined at an r value of 0 in $p(r)$. The radius of the gyration (R_g) could be calculated by the following equation, eq 1.[25]

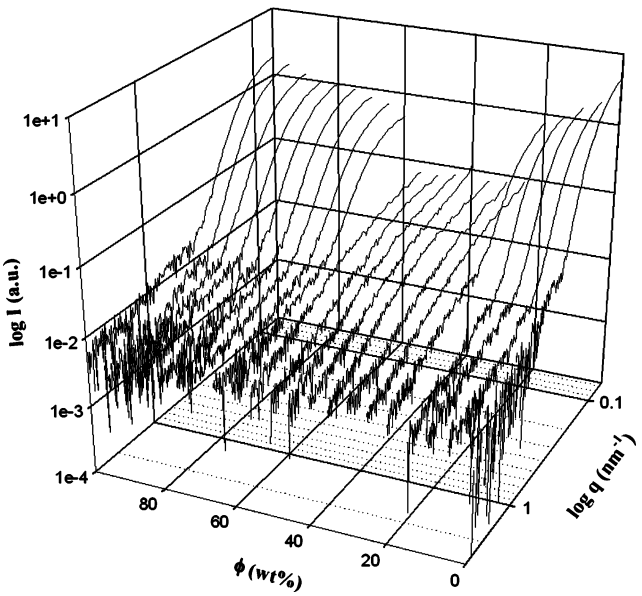

Figure 1. SAXS curves of 1 wt % PS(12K)-*b*-P4VP(11.8K) solutions, as functions of q and ϕ.

$$R_g = \frac{\int r^2 p(r)}{2\int p(r)} \quad (1)$$

Results and Discussion

Figure 1 shows the SAXS curves as functions of q and ϕ. The SAXS intensity of solutions decreased from those of pure toluene, as the ϕ increased to $\phi = 20$, and then dropped suddenly to a low level (the isotropic state) at $\phi = 25-60$. It appeared stepwise at $\phi = 65$, and increased again until $\phi = 100$. Toluene and ethanol are selective solvents for PS and P4VP, respectively, so the micelle core between $\phi = 0$ and 20 was P4VP and that between $\phi = 65$ and 100 was PS. The selectivity of the mixed solvent deteriorated when toluene was mixed with ethanol (or visa versa), and the isotropic state was found in the central regions between $\phi = 25$ and 60.

Figure 2 shows $p(r)$, D_{max}, R_g, and $I(0)$ in which $p(r)$ was calculated from Figure 1, and D_{max}, R_g, and $I(0)$ were calculated from $p(r)$. The $p(r)$s (Figure 2a) represented the typical shape of a spherical micelle although the intensity decreased by mixing with the other solvent, indicating that the basic shape of the individual micelles did not change, but the aggregation number in the micelles decreased (this will be discussed later in this paragraph). Figure 2b shows the plots of D_{max}, and R_g with respect to ϕ. The D_{max} overlapped with R_g in the difference scale in Figure 2b. The D_{max} was approximately 2.93 times higher than the R_g, which was calculated from the linear curve fitting of the D_{max} plot vs the R_g. If the micelle was a homogeneous sphere, the ratio between the D_{max} and the R_g would be 2.58 ($2 \times \sqrt{5}/3$). The fact that the observed D_{max}/R_g (2.93) was larger than that of the theoretical homogeneous one (2.58) might be due to a core/shell structure in the micelle. The isotropic state was observed below $D_{max} = 29$ nm. The interfacial tension decreased and the stretched core chains were

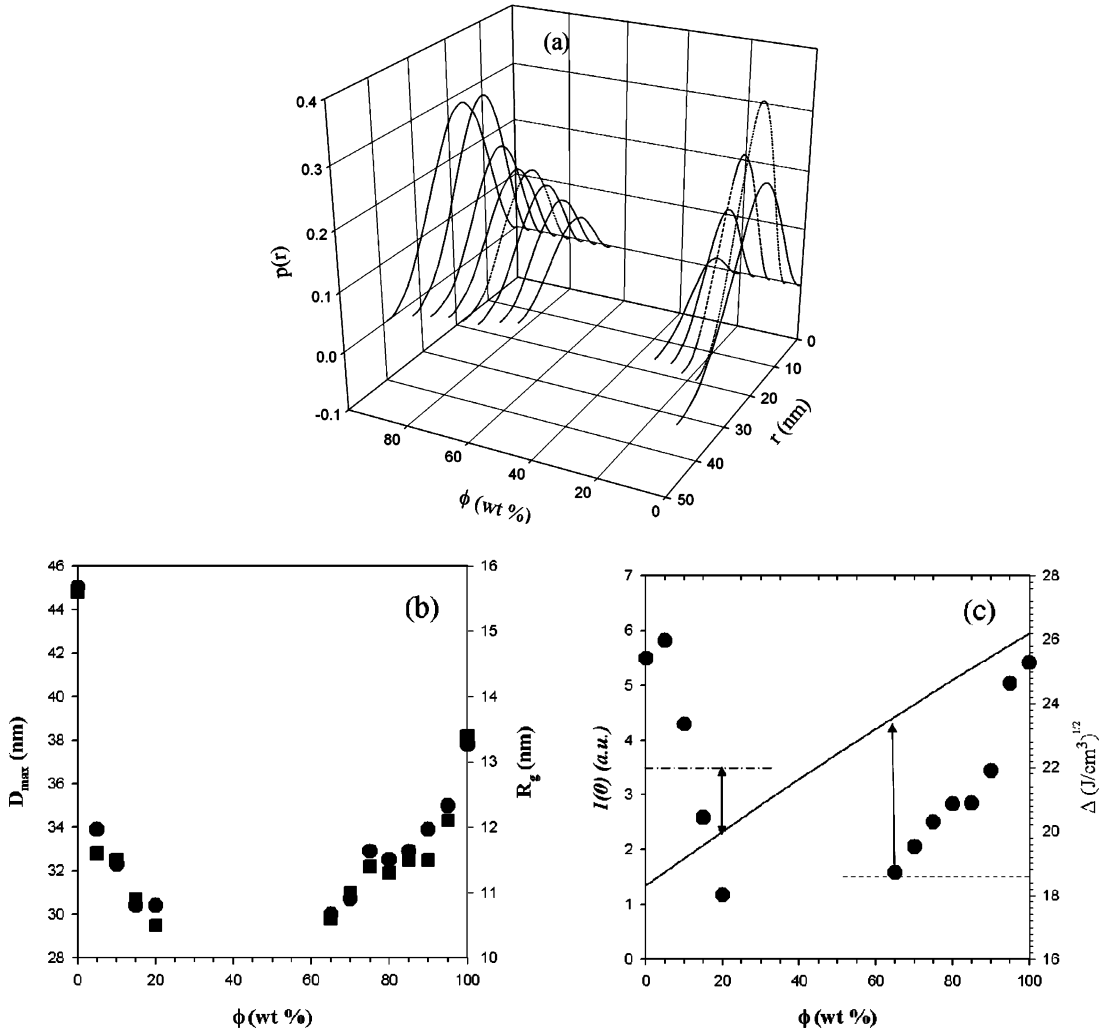

Figure 2. (a) $P(r)$, (b) D_{max} (■) and R_g (●), and (c) $I(0)$ of a 1 wt % PS(12K)-*b*-P4VP(11.8K) solution with respect to ϕ; $p(r)$ was calculated from Figure 1, and D_{max}, R_g, and $I(0)$ were calculated from $p(r)$; the —, ---, and —·— lines in Figure 2c represent the solubility parameters of solvent mixtures, PS, and P4VP, respectively.

relaxed by a decrease in the selectivity of the solvent mixtures. The relaxed chains in the core caused loss of integration between chains and thus, resulted in the isotropic state at a certain size. This size for PS(12K)-*b*-P4VP(11.8K) seemed to be at $D_{max} =$ 29 nm. Figure 2c shows $I(0)$ with respect to ϕ. The $I(0)$ was known to be in proportion with the aggregation number of the micelle (Z). It is possible for the micelle to be swollen by the selective solvent. The core of a micelle in the less-selective solvent likely contains more solvent. If solvent is left in the core, the scattering from the micelle also decreases because small-angle X-ray scattering comes from electron density difference between the solvent and the core. Thus, the small-angle X-ray scattering is closely proportional to the number of the block copolymers in the micelle although swelling of the core is also considered. The $I(0)$ (and Z) decreased by ~83% in maximum due to mixing with the other solvent. This drop in Z was large compared with the decrease in micelle size; the size of the micelle dropped from 46 to 29 nm (in maximum), therefore the volume decreased by ~75%. Thus, the micelles in the less selective solvent were softer than those in the high-selective solvent. It was interesting that the size and hardness of the micelle could be controlled by mixing the two solvents, which had different selectivities.

Table 1 is a summary of solubility parameters of PS, P4VP, ethanol, and toluene. The solubility parameter of toluene (18.3 $(J/cm^3)^{1/2}$) is nearly the same as that of PS (18.6 $(J/cm^3)^{1/2}$),

Table 1. Summary of Solubility Parameters $(J/cm^3)^{1/2}$

PS[a]	18.6
P4VP[a]	~22
toluene[b]	18.3
ethanol[b]	26.2

[a] *J. Polym. Sci., Polym. Chem.* **1985**, *23*, 1099−1108. [b] *Handbook of solubility parameter*; CRC Press: Boca Raton, FL, 1983.

indicating that PS is completely soluble in toluene. The solubility parameter of ethanol (26.2 $(J/cm^3)^{1/2}$) is close to that of P4VP (22 $(J/cm^3)^{1/2}$) while the difference in the solubility parameter between ethanol and P4VP (4.2 $(J/cm^3)^{1/2}$) is larger than that between toluene and PS (0.3 $(J/cm^3)^{1/2}$). The solubility parameters of the mixtures can be calculated by the mixing rule in volume ratio. The solid line in Figure 2c represents the solubility parameter of the solvent mixture, and it is a little curved due to the difference in density between toluene and ethanol. The arrows in Figure 2c represent the solubility parameter difference (Δ) between the core block and the mixture solvent at the starting points of the isotropic state (at $\phi = 20$ wt % and 65 wt %). The arrow on the right side in Figure 2c is for the Δ_{PS} between the PS core and the solvent mixture at $\phi =$ 65 wt %. The arrow on the left side is for the Δ_{P4VP} between the P4VP core and the solvent mixture at $\phi = 20$ wt %. The Δ_{PS} was approximately 5 $(J/cm^3)^{1/2}$. However, the Δ_{P4VP} was approximately 2 $(J/cm^3)^{1/2}$, which is smaller than the Δ_{PS} (5 $(J/cm^3)^{1/2}$). The solubility parameter of the P4VP in Table 1

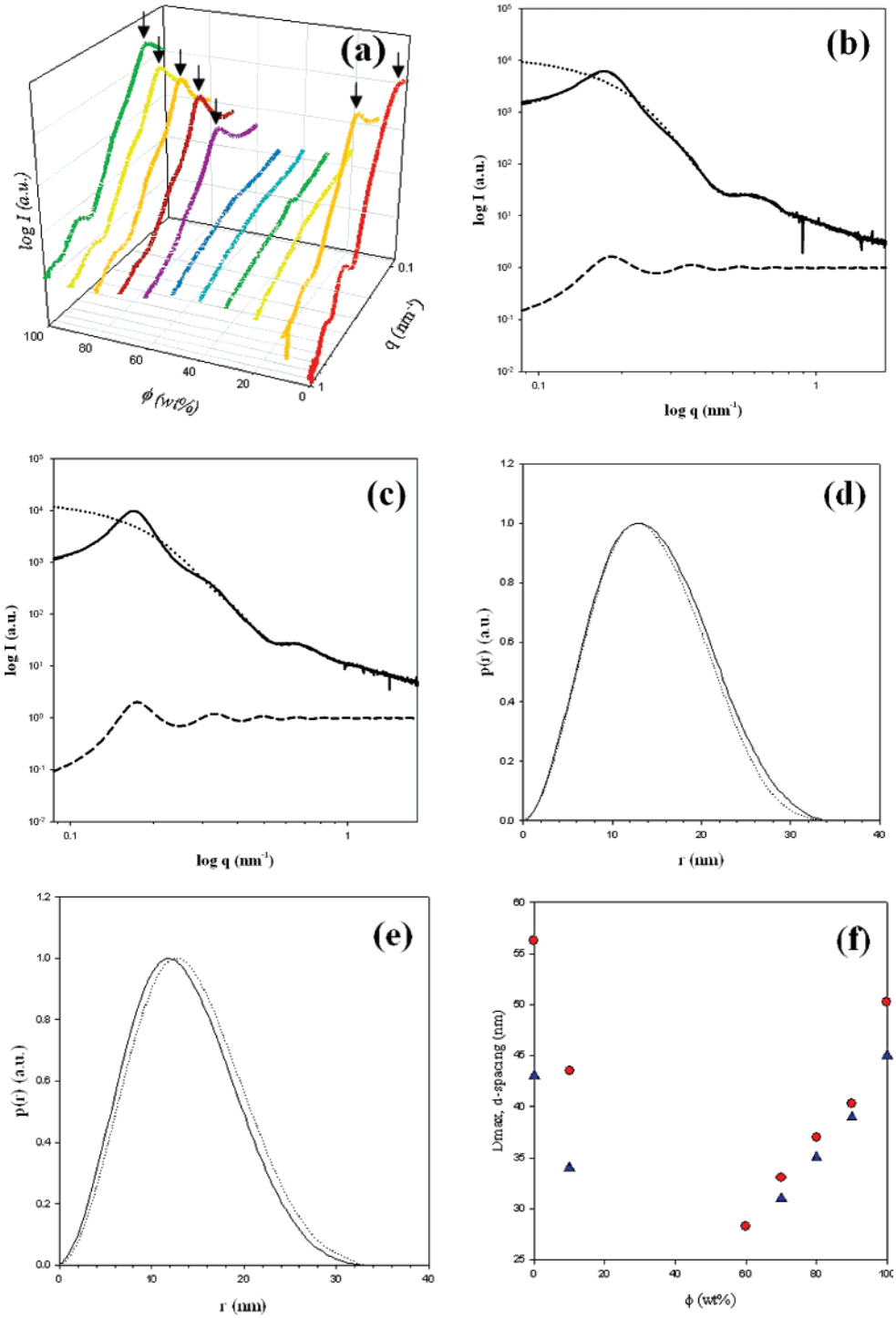

Figure 3. (a) SAXS curves of 8 wt % PS(12K)-*b*-P4VP(11.8K) solutions, as functions of q and ϕ and the arrows represent q_{max} (the q value at maximum intensity); the observed (solid line) and calculated (−···−) SAXS patterns of 8 wt % solutions with the form (···) and structure (− −) factors at $\phi = 10$ (b) and $\phi = 80$ (c); the normalized $p(r)$s at $\phi = 10$ (d) and 80 (e) in which solid and dotted lines are for 1 (Figure 2a) and 8 wt % solutions, respectively;. (f) d-spacing of the q_{max} (red ●) and D_{max} (blue ▲).

(~22 $(J/cm^3)^{1/2}$) was calculated by using the group contribution method.[32−34] To our knowledge, there have not been any reports of experimental data for the solubility parameter of P4VP. There is a significant possibility that the solubility parameter of P4VP has a higher value when considering the small Δ_{P4VP} (in our data) and the highly segregated regime of PS-*b*-P4VP, which shows a large difference in the solubility parameter between the two blocks. Such details, however, are outside the scope of this study.

Figure 3a shows the SAXS curves of 8 wt % solutions as functions, of q and ϕ. The intensity was low and flat at the central regions of ϕ, indicating that these regions were in the isotropic state. Here, 50 wt % of toluene and 30 wt % of ethanol were needed to obtain an isotropic state from pure ethanol and toluene solutions, respectively. This result strongly suggested that ethanol was a more selective solvent for P4VP than toluene for PS. The structure factor appeared due to a decrease in intensity at a low q, and this caused the appearance of a peak, as shown in the arrows of Figure 3a. Parts b and c of Figure 3, for example, show the observed and calculated SAXS patterns of 8 wt % solutions at $\phi = 10$ and 80, respectively, with the form and structure factors that were separated using the GIFT

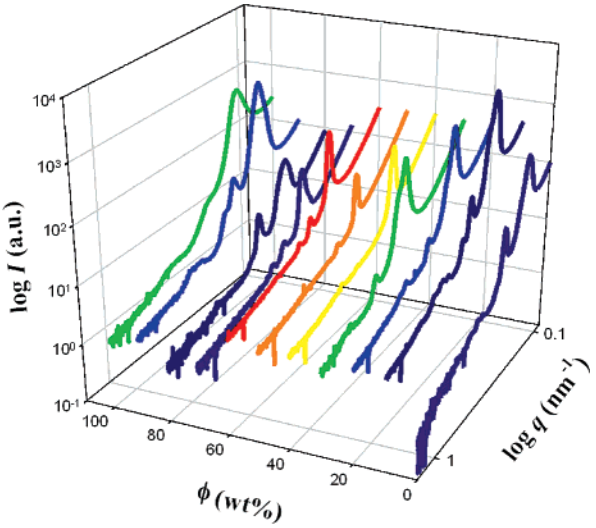

Figure 4. SAXS curves of 16 wt % PS(12K)-*b*-P4VP(11.8K) solutions, as functions of q and ϕ.

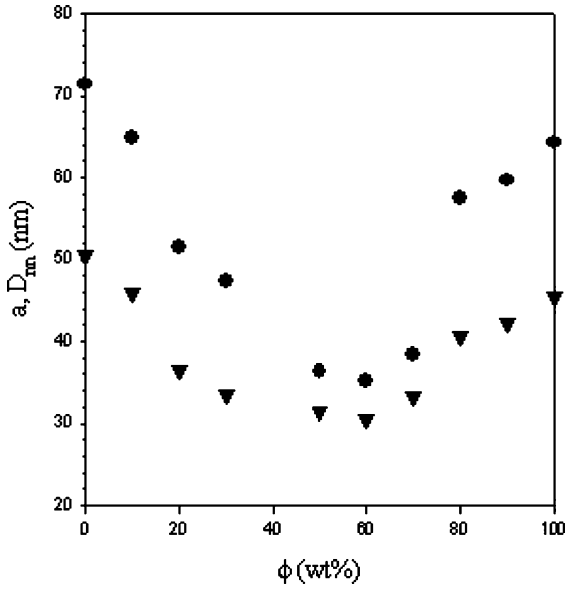

Figure 5. a dimension and D_{nn}, with respect to ϕ: a (●) and D_{nn} (▼).

method. The observed and calculated curves are so close each other that they are hard to be distinguished, indicating that the form and structure factors were accurately separated from the observed SAXS pattern. Parts d and e of Figure 3 show the normalized $p(r)$s of 1 (Figure 2a) and 8 wt % solutions at $\phi =$ 10 and 80, respectively. The $p(r)$s of the 8 wt % solutions (dotted line) were calculated by the form factors in Figure 3, parts b and c, and were compared with the $p(r)$s of 1 wt % solutions (solid line), which had only form factors, as shown in Figure 2. The $p(r)$s were similar to each other (between 1 and 8 wt % solutions) although small differences existed, indicating that the basic micelle structure did not change by an increase in concentration from 1 to 8 wt %. Similar results were found for the results from different ϕ's. The d-spacing of the peak position defines the average distance between micelles. Figure 3f shows a comparison between the d-spacing of q_{max} and D_{max}. The d-spacing of q_{max} was a little higher than D_{max}. The closeness between the d-spacing of q_{max} and D_{max} indicates that the micelle was almost space-filling in the 8 wt % solution.

Figure 4 shows SAXS curves of 16 wt % solutions, as functions of q and ϕ. Several peaks appeared as the concentration increased to 16 wt %. Table 2 shows observed q values

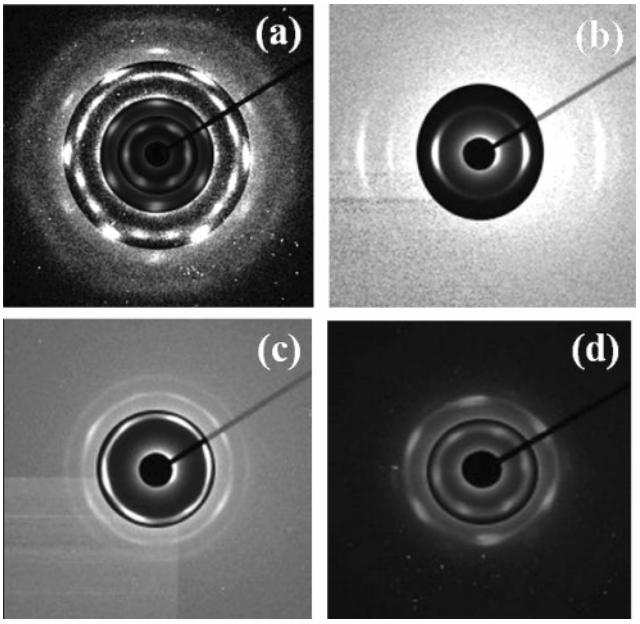

Figure 6. Two-dimensional SAXS patterns of 16 wt % solutions shearing between mica films, in the vertical direction at (a) $\phi = 0$, (b) $\phi = 40$, (c) $\phi = 60$, and (d) $\phi = 100$. The contrast of the central part was modified to better distinguish between reflections.

and their ratios. The symmetries of the unit cells in Table 2 were determined from their ratios. The solutions in the high-selective solvents (such as $\phi = 0$, 10, 20, 30, 80, 90, and 100) demonstrated fcc symmetry, although solutions in less selective solvents (such as $\phi = 50$, 60, and 70) showed bcc symmetry. From the dilute solutions, we found that the micelles from the high-selective solvents were larger and harder than those of the less-selective solvents. Watzlawek et al. also found a transition from fcc to bcc at a certain range of the packing fraction from the Monte Carlo calculation of a star polymer solution. This was done by increasing the arm number (i.e., an increasing in the hardness of the star polymer).[35] The solution at $\phi = 40$ showed several peaks with hexagonal symmetry ratios of 1:2: $\sqrt{7}$; the peak at $\sqrt{3}$ ratio was missing due to weak intensity. Hexagonal symmetry should contain cylindrical units in the unit cell, which means that the micelles (or basic units) were not spherical but cylindrical. Cylindrical micelle will be discussed later in this paper via TEM images. Lamella is not ruled out for a possible structure at certain ϕs in the neutral solvent because 10 intervals in ϕ may be not narrow enough for the complete screening of the solvent-mixture ratios. Thermodynamically stable lamella were also found in the solid-state structure, which was obtained when the solvent was evaporated from the 16 wt % solution (will be discussed in a later part of this paper).

Figure 5 shows the a dimension of the cubic structure and D_{nn} (the closest distance between micelles in the unit cell), with respect to ϕ.[24] The a dimension showed discontinuity between fcc and bcc symmetries at $\phi = 80$, although the D_{nn} was almost parabolic with respect to ϕ. The a dimension of the hexagonal lattice at $\phi = 40$ was similar to that of the cubic lattice at $\phi =$ 50, 60, and 70. It is interesting that the D_{nn} curve was flat at $\sim$ 30 nm in the central regions of ϕ ($\phi = 30-70$). This value was close to the minimum D_{max} value ($\sim$29 nm) in Figure 2. This result also suggests that the size of the micelles had a lower limit of $D_{max} = \sim$ 29 nm for PS(12K)-*b*-P4VP(12K) even in the concentrated solutions.

Parts a and d of Figure 6 show the two-dimensional SAXS patterns of the 16 wt % solutions shearing in the vertical

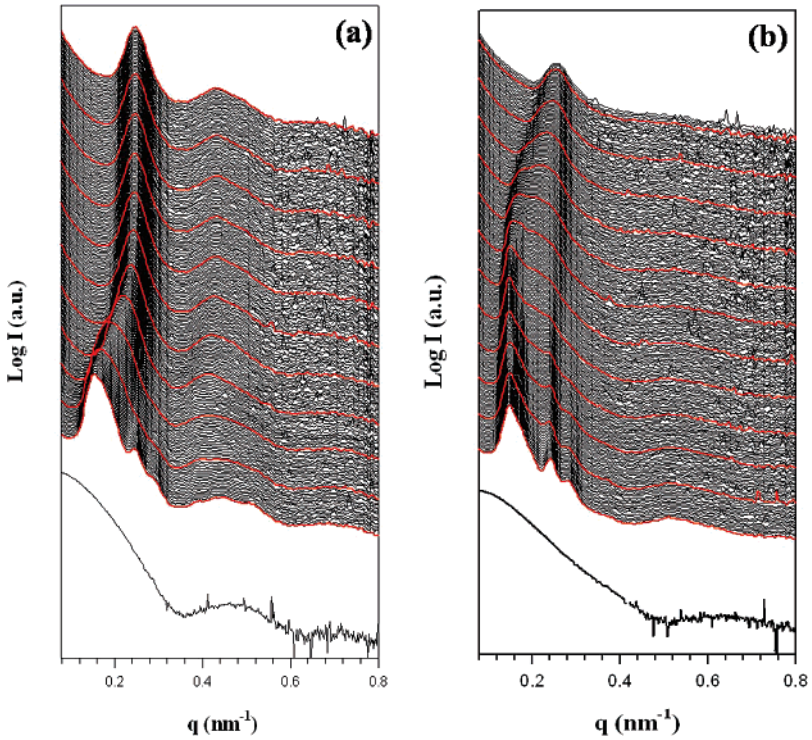

Figure 7. SAXS curves of PS(12K)-*b*-P4VP(11.8K) at $\phi = 0$ (a), and 100 (b) during evaporation from the 16 wt % solution to a solid state; the red curves were at 100 s interval; the bottom curve is the scattering from the 1 wt % solution, for comparison.

Table 2. Ratios of q/q_{first} (q_{first} is the q Value of the First Peak), Symmetries (fcc, Face Centered Cubic; bcc, Body Centered Cubic; Hex, Hexagonal), a Dimension, and D_{nn} (the Closest Distance between Micelles in the Unit Cell), Which Were Calculated from the Observed q Values in Figure 4

ϕ (wt %)	ratios of q/q_{first}	q_{first} (nm^{-1})	symmetry	a (nm)	D_{nn} (nm)
0	1:2/√3:√8/3:√11/√3:√20/√3:√24/√3:√32/√3	0.1523	fcc	71.38	50.47
10	1:2/√3:√8/√3:√11/√3:√20/√3:√24/√3:√32/√3:√35/√3	0.1681	fcc	64.88	45.83
20	1:2/√3:√8/√3:√11/√3:√24/√3	0.2116	fcc	51.54	36.43
30	1:2/√3:√8/√3:√19/√3	0.23	fcc	47.39	33.51
40	1:2:√7	0.2096	Hex	35.07	
50	1:√2	0.2453	bcc	36.27	31.4
60	1:√2:√3	0.2373	bcc	35.21	30.49
70	1:√2:√3	0.2314	bcc	38.47	33.32
80	1:√8/√3	0.1899	fcc	57.44	40.61
90	1:√8/√3:√11/√3	0.1839	fcc	59.67	42.19
100	1:√8/√3	0.1681	fcc	64.23	45.41

direction between mica films at $\phi = 0$ and 100. The six inner peaks in both patterns were a result of hexagonal closely packed layers. Layers of hexagonally packed micelles were aligned to the surface of the mica film. The presence of six inner reflections indicates that the stacking sequence of layers of the hexagonally packed micelles could not be purely ABCABC.... as in a fcc structure, but had to include sequences of ABAB... stacking, as in a hexagonal closely packed structure, thus indicating a hcp/fcc random structure.[36−42] Figure 6b shows two-dimensional SAXS patterns of the concentrated solutions (16 wt %) at $\phi =$ 40. Several equatorial reflections were observed at $q = 0.2096$, 0.4154, and 0.5558 nm^{-1}. Their ratios were 1:2:√7 and they were well matched with hexagonal symmetry, as seen in Table 2 and Figure 4. The reflections were observed only on the equator and could be indexed as *hk*0, which also indicated the two-dimensional hexagonal unit cell. Figure 6c shows the two-dimensional SAXS patterns of the concentrated solutions (16 wt %) at $\phi = 60$. The ratios of the observed q values were 1:√2:√3, indicating that the micelles were packed into a bcc unit cell. This two-dimensional pattern was quite similar to the twinned bcc patterns observed by other scientists.[43−46]

Figure 7a shows changes in the SAXS curves during evaporation from the 16 wt % toluene solution to the solid state. The bottom curve is the scattering from the 1 wt % toluene solution, for comparison, which shows only the form factor. The initial scattering curves were identical to Figure 4 ($\phi = 0$) (showing fcc symmetry). The first and second maxima of the form factor at $q = \sim 0.46$ and ~ 0.7 nm^{-1} were also observed, respectively. The shapes and positions of these maxima were well matched with the scattering from the 1 wt % solution (the bottom curve) and were maintained during drying. The overlapping of the spherical form factor with reflections indicates that the spherical micelles were still the basic structural units in the concentrated solution. The first reflection of the fcc symmetry at $q = 0.152$ nm^{-1} continuously shifted to a high q and was broadened until an evaporation time (t_{evap}) of 460 s during drying. The scattering curves after $t_{evap} = 460$ s did not change due to complete drying and they showed a broad reflection at $q = \sim 0.25$ nm^{-1} (d-spacing = 25.1 nm) with two broad maxima at $q = \sim 0.46$ and ~ 0.7 nm^{-1} (which were from the form factor). The fact that a broad reflection overlapped with the form factor indicates that the micelle was the basic unit even for the dried film, similar to the concentrated solution, and only a short-range order existed between micelles, which was confirmed by the TEM study (will be discussed later). Figure 7b shows the SAXS curves for the evaporation of the ethanol solution. The initial

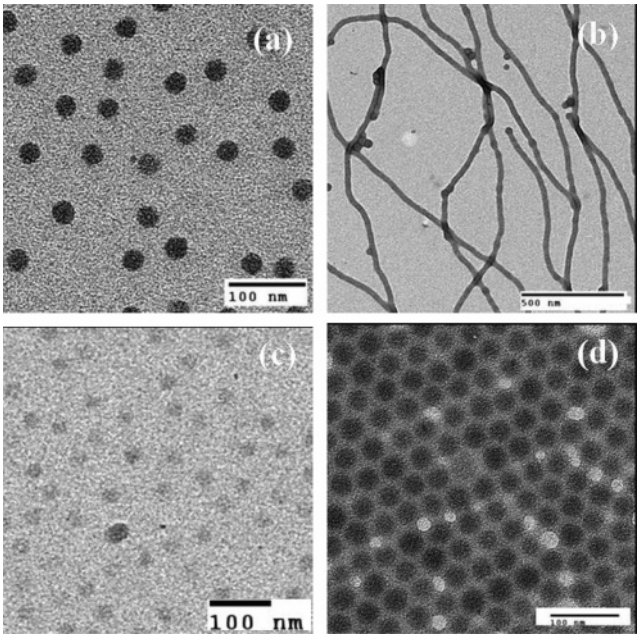

Figure 8. TEM images of PS(12K)-*b*-P4VP(11.8K) at (a) $\phi = 0$, (b) 40, (c) 60, and (d) 100, which were prepared by the evaporation of the 0.016 wt % solutions on the carbon-coated copper grid, and stained with I_2.

scattering curves were identical to Figure 4 ($\phi = 100$), showing fcc symmetry. Similar to the toluene solution, only a short-range order existed after drying, which could be also insinuated from a single broad reflection at $q = 0.26$ nm^{-1} (d-spacing = 24.2 nm) and the disappearance of other high-order reflections during drying.

Figure 8 shows TEM images from the samples, which were prepared by evaporation of the 0.016 wt % solutions on the carbon-coated copper grid. This sample preparation method for TEM could not control the concentration of the solid state because the concentration of the solution became dense during the evaporation of the solvent on the grid. In addition, the equilibrium structures could not be observed due to the high speed of toluene and ethanol evaporation. Information, however, can be obtained for the kinds of the structures present in the PS-*b*-P4VP. Spherical micelles were observed from high selective solutions at $\phi = 0$ and 100 while cylindrical micelles were observed from the isotropic solution at $\phi = 40$. These cylindrical micelles were generated from the isotropic state, by condensing solvents during evaporation on the carbon-coated grid. Zhao et al. studied the effects of substrate, solvent, and concentration on the surface topography of thin PS-*b*-P4VP films made from a neutral solvent.[47] They found cylindrical micelles of PS(21.4K)-*b*-P4VP(20.7K) on the graphite substrate from a neutral chloroform solution, which were dependent upon concentration, substrate, and composition. Spatz et al. hypothesized that for the PS-*b*-P2VP system using the nonselective solvent chloroform, hydrophobic substrates allowed for the generation of hydrophilic islands;[48] however, in their experiment, only a strip-like structure was found rather than islands. They thought that the difference in $\pi-\pi$ interactions between the blocks and the graphite, and that in the interfacial energies between PS and P4VP contributed to the formation of cylindrical micelles on graphite. More studies regarding cylindrical micelle are needed for better clarification, although it is obvious that the cylindrical micelles of PS(12K)-*b*-P4VP(11.8K) could be formed by controlling solvent selectivity. Figure 8c shows TEM images at $\phi = 60$. Fuzzy, spherical micelle images were observed. The

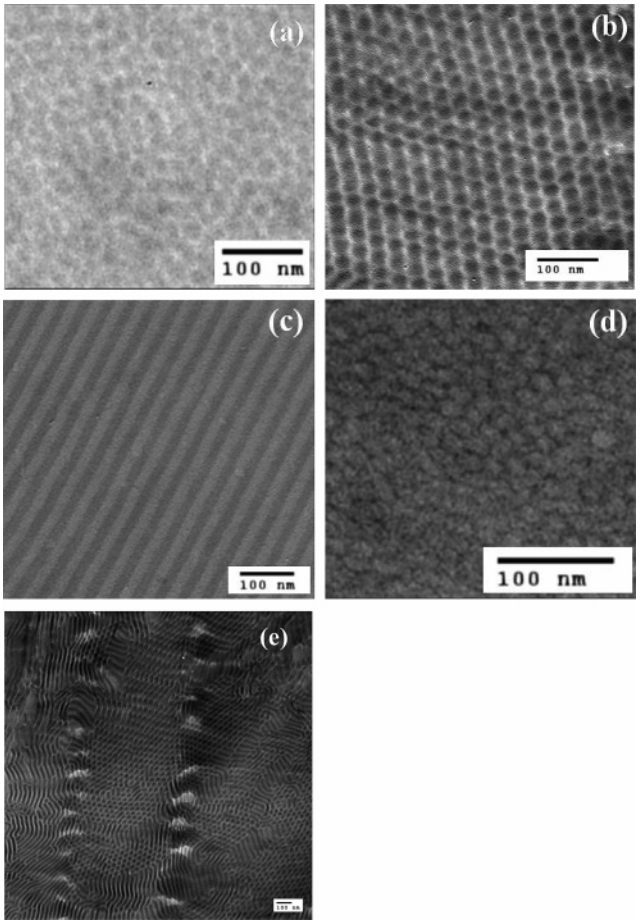

Figure 9. TEM images of the 16 wt % solution films at $\phi =$ (a) 0, (b) 40, (c) 50, and (d) 100, which were completely dried between PET films (for slow drying), microsectioned along the film thickness direction, and stained with I_2. (e) TEM image of the misaligned part of image b.

shallow darkness in the micelles indicates that soft micelles were generated due to less selectivity of the solvent.

Parts a and d of Figure 9 show TEM images of the films of the 16 wt % solutions at $\phi = 0$ and 100, respectively, which were completely dried between the PET films (for slow drying), microsectioned along the film thickness direction, and stained with I_2. The micelles were randomly packed without any symmetry. The corona and core parts of the micelles were stained for ethanol and toluene solutions, respectively, due to the P4VP location; I_2 selectively stained P4VP. The average distance between micelles in Figure 9, parts a and d, was approximately 25 nm. These values were in accordance with the d-spacings of the main broad peak (~25 nm) in Figure 7, supporting that the broad peak observed from SAXS was due to the short-range order between micelles. Figure 9b shows a TEM image of the sample from the solution at $\phi = 40$, which was sectioned perpendicular to the sheared direction. Hexagonal packing was observed in the concentrated solution at $\phi = 40$ from SAXS. Well-ordered hexagonal packing was observed with the dimension of $a = 34$ nm, which was in accordance with the X-ray results (see Table 2). Figure 9e shows the misaligned part of the sectioned film demonstrating a long cylinder with hexagonal packing. The hexagonal packing in the concentrated solution is well maintained after drying. The core part of the cylinder was darker in the TEM image (Figure 9b,e), which is perhaps due to a little more PS selectivity in the solvent at $\phi =$ 40. Figure 9c represents the sample from the solution at $\phi =$ 50, showing a well-ordered lamellar structure. The total layer

thickness was 38 nm whereby the PS and P4VP parts were 20 and 18 nm thick, respectively. The lamellar structure was a double layered one with each layer consisting of two block units ($-$(P4VP$-$P4VP$-$PS$-$PS)$_n-$). This is because the layer thickness (38.3 nm) was a little smaller than twice that of the most extended chain length (22.6 nm).[24] The lamellar structure is the most thermodynamically stable for PS(12K)-*b*-P4VP(11.8K) due to the similar block length between PS and P4VP. PS(12K)-*b*-P4VP(11.8K) was formed into a soft spherical micelle with bcc symmetry in 16 wt % solution at $\phi = 50$, as discussed in Figure 4 and Table 2. These soft spherical micelles could be easily transformed into the thermodynamically stable lamellar structures, however, hard and large micelles in the highly selective solvents might be too stable to transform into the lamellar structures, as shown in Figure 9, parts a and d.

Conclusions

The structures of PS(12K)-*b*-P4VP(11.8K) were strongly dependent on solvent selectivity and the concentration of the solution. We could finely tune the various structures for PS(12K)-*b*-P4VP(11.8K), such as hard/soft spherical micelles in the dilute solution, fcc, bcc, and hexagonal packing in the concentrated solution, and randomly packed micellar, lamellar, and hexagonal structures in the solid state by using toluene/ethanol mixtures in this study. The individual spherical micelles were observed in a dilute solution (1 wt %) at $\phi = 0$ to 20, and 70 to 100, while isotropic states were found in other solvent mixture ratios. The core size and the aggregation number of the micelles continuously decreased by mixing with the other solvent until the D_{max} was 29 nm. The hard and large spherical micelles were formed at high-selective solvent mixtures, while the soft and small ones were formed at less-selective solvent mixtures. The micelles were close enough to show the structure factor in a semidilute solution (8 wt %) although basic micelles barely changed. The new soft micelles, which were in the isotropic state in the nonselective solvents, were formed by increasing the concentration to 16 wt %. The micelles were packed in a cubic lattice at the concentrate solution (16 wt %) in the entire solvent mixture, except for the solution at $\phi = 40$, which had two-dimensional hexagonal packing. The hard micelles favored fcc symmetry although soft micelles favored bcc symmetry. In the solid state which was prepared by evaporating a 16 wt % solution, the structures were strongly dependent on the stability of the already existing micelles. The hard spherical micelles in the high-selective solvents and the hexagonally packed structure at $\phi = 40$ were maintained, although soft micelles in the less-selective solvent ($\phi = 50$) were transformed into a thermodynamically stable lamellar structures. The hard spherical micelles in the highly selective solvents, however, lost their long-range order and were randomly packed in a solid state.

Acknowledgment. This work was supported by the Korea Research Foundation Grant funded by the Korean Government (MOEHRD, Basic Research Promotion Fund) (KRF-2006-311-D00426). And synchrotron work was supported in part by the Ministry of Science & Technology (MOST), by POSCO, by the Center for Integrated Molecular System (Korea Science & Engineering Foundation), by the KISTEP (Basic Research Grant of Nuclear Energy, MOST).

References and Notes

(1) Hadjichristidis, N.; Pispas, S.; Floudas, G. *Block Copolymers: Synthetic Strategies, Physical Properties and Applications*; Wiley: New York, 2003.
(2) Tuzar, Z.; Kratochvil, P. *Adv. Colloid Interface Sci.* **1978**, *6*, 201.
(3) Liu, G.; Ding, J.; Guo, A.; Herfort, M.; Bazett-Jones, D. *Macromolecules* **1997**, *30*, 1851.
(4) Yan, X.; Liu, F.; Li, Z.; Liu, G. *Macromolecules* **2001**, *34*, 9112.
(5) Jenekhe, S. A.; Chen, X. L. *Science* **1999**, *283*, 372.
(6) Liu, G.; Qiao, L.; Guo, A. *Macromolecules* **1996**, *29*, 5508.
(7) Zhang, L.; Eisenberg, A. *Macromolecules* **1996**, *29*, 8805.
(8) Borisov, O. V.; Zhulina, E. B. *Macromolecules* **2003**, *36*, 10029.
(9) Zhou, Z.; Li, Z.; Ren, Y.; Hillmyer, M. A.; Lodge, T. P. *J. Am. Chem. Soc.* **2003**, *125*, 10182.
(10) Zhang, L.; Eisenberg, A. *Science* **1995**, *268*, 1728.
(11) Zhang, L.; Eisenberg, A. *Macromolecules* **1996**, *29*, 8805.
(12) Van, der Maarel, J. R. C.; Groenewegen, W.; Egelhaaf, S. U.; Lapp, A. *Langmuir* **2000**, *16*, 7510.
(13) Yu, Y.; Eisenberg, A. *J. Am. Chem. Soc.* **1997**, *119*, 8383.
(14) Ding, J.; Liu, G. *Macromolecules* **1999**, *32*, 8413.
(15) Zhang, L.; Eisenberg, A. *Science* **1995**, *268*, 1728.
(16) Shen, H.; Eisenberg, A. *J. Phys. Chem. B* **1999**, *103*, 9473.
(17) Chen, L.; Shen, H.; Eisenberg, A. *J. Phys. Chem. B* **1999**, *103*, 9488.
(18) Zhang, L.; Eisenberg, A. *Macromolecules* **1999**, *32*, 2239.
(19) Shen, H.; Eisenberg, A. *Macromolecules* **2000**, *33*, 2561.
(20) Choucair, A.; Eisenberg, A. *Eur. Phys. J. E* **2003**, *10*, 37.
(21) Antonietti, M.; Heinz, S.; Schmidt, M.; Rosenauer, C. *Macromolecules* **1994**, *27*, 3276$-$81.
(22) Bossé, F.; Schreiber, H. P.; Eisenberg, A. *Macromolecules* **1993**, *26*, 6447.
(23) Calderara, F.; Riess, G. *Macromol. Chem. Phys.* **1996**, *197*, 2115.
(24) Park, S. -Y.; Chang, Y. J.; Farmer, B. L. *Langmuir* **2006**, *22*, 11369.
(25) Glatter, O.; Krathy, O. *Small-Angle X-ray Scattering*; Academic Press: London, 1982; p 126.
(26) Glatter, O. *J. Appl. Crystallogr.* **1997**, *10*, 415.
(27) Glatter, O. *J. Appl. Crystallogr.* **1980**, *13*, 577.
(28) Glatter, O. *J. Appl. Crystallogr.* **1981**, *14*, 101.
(29) Brunner-Popela, J.; Glatter, O. *J. Appl. Crystallogr.* **1997**, *30*, 431.
(30) Bergmann, A.; Fritz, G.; Glatter, O. *J. Appl. Crystallogr.* **2000**, *33*, 1212.
(31) Weyerich, B.; Brunner-Popela, J.; Glatter, O. *J. Appl. Crystallogr.* **1999**, *32*, 197.
(32) Coleman, M. M.; Graf, J. F.; Painter, P. C. *Specific interactions and the miscibility of polymer blends*; Technomic Publishing: Lancaster, PA, 1991.
(33) Mangaraj, D.; Bhatnagar, S. K.; Rath, S. B. *Makromol. Chem.* **1963**, *67*, 75.
(34) Kuo, S. W.; Lin, C. L.; Chang, F. C. *Polymer* **2002**, *43*, 3943.
(35) Watzlawek, M.; Likos, C. N.; Löwen, H. *Phys. Rev. Lett.* **1999**, *82*, 5289.
(36) McConnell, G. A.; Lin, M. Y.; Gast, A. P. *Macromolecules* **1995**, *28*, 6754.
(37) Hamley, I. W.; Pople, J. A.; Fairclough, J. P. A.; Ryan, A. J.; Booth, C.; Yang, Y. -W. *Macromolecules* **1998**, *31*, 3906.
(38) Hamley, I. W.; Pople, J. A.; Diat, O. *Colloid Polym. Sci.* **1998**, *276*, 446.
(39) Ackerson, B. J. *J. Rheol.* **1990**, *34*, 553.
(40) Dux, C.; Versmold, H.; Reus, V.; Zemb, T.; Lindner, P. *J. Chem. Phys.* **1996**, *104*, 6369.
(41) Dux, C.; Musa, S.; Reus, V.; Versmold, H.; Schwahn, D.; Lindner, P. *J. Chem. Phys.* **1998**, *109*, 2556.
(42) Clarke, S. M.; Rennie, A. R.; Ottewill, R. H. *Langmuir* **1997**, *13*, 1964.
(43) Almdal, K.; Koppi, K. A.; Bates, F. S. *Macromolecules* **1993**, *26*, 4058.
(44) McConnell, G. A.; Lin, M. Y.; Gast, A. P. *Macromolecules* **1995**, *28*, 6754.
(45) Park, M. J.; Bang, J.; Harada, T.; Cha, K.; Lodge, T. P. *Macromolecules* **2004**, *37*, 9064.
(46) Mortensen, K.; Theunissen, E.; Kleppinger, R.; Aldmal, K.; Reynaers, H. *Macromolecules* **2002**, *35*, 7773.
(47) Zhao, J.; Tian, S.; Wang, Q.; Liu, X.; Jiang, S.; Ji, X.; An, L.; Jiang, B. *Eur. Phys. J. E* **2005**, *16*, 49.
(48) Spatz, J. P.; Sheiko, S.; Moller, M. *Adv. Mater.* **1996**, *8*, 513.

MA0700072